Design, Molecular Dynamics and Battery Performance Studies of the Electrolyte Molecule $C_6Li_6O_3$

Annadurai V[1], R Gopalkrishne Urs[2], R Somashekar[3]
[1,2]*Department of Physics, NIE First Grade College, University of Mysore, Mysore-570 008, Karnataka, India*
[3]*Department of Studies in Physics, University of mysore, Manasagangotri, Mysore -570 006, Karnataka, India.*

***Abstract*—To enhance electrolyte performance in lithium-ion batteries, we designed a novel molecule, $C_6Li_6O_3$, with strategically arranged lithium atoms to maximize Coulombic efficiency and improve cycle life. This configuration was analyzed using molecular modeling and Molecular Dynamics (MD) simulations. By integrating computational tools with the molecule's 3D structure, we calculated essential properties of $C_6Li_6O_3$, including ionic conductivity, diffusivity, density, viscosity, and thermal conductivity. Using PyBaMM software, we conducted detailed battery simulations, monitoring the electrolyte's behavior over 3,600 seconds. The resulting voltage-time, voltage-capacity, and current-time profiles demonstrate enhanced electrochemical performance and durability, highlighting the electrolyte's improved properties. Our findings indicate that $C_6Li_6O_3$ has substantial potential to drive advancements in high-performance, long-life electrolytes, representing a promising step toward the next generation of materials for battery applications.**

***Index Terms*—$C_6Li_6O_3$, Electrolyte, Battery, Molecular Dynamics**.

I. INTRODUCTION

The development of next-generation batteries increasingly focuses on lithium-based materials, attracting considerable attention to the role of lithium atoms in performance enhancement [1-4]. Modeling molecules that influence the physical and chemical properties of materials may provide an effective approach to designing high-performance electrolytes [5]. There is sustained interest in creating new electrolytes to improve the performance of lithium-based batteries [6, 7]. Numerous studies have utilized molecular dynamics simulations to explore electrolyte properties, particularly to enhance lithium-ion energy storage [8], investigate the effect of lithium on the tensile behaviour of BCC iron [9], study lithium diffusion mechanisms [10], analyze lithium-ion transport [11, 12], simulate lithium-ion battery reactivity [13], and examine lithium-ion conduction at grain boundaries [14]. In previous work, we designed and analyzed the molecule Li_6O_6 for its crystal structure and battery properties, which showed limited promise [15]. Figure-1 shows the chemical structure of Li_6O_6 molecule. In the present study, we adopt a new approach by designing a novel molecule which has a similar chemical structure with different atoms, characterizing it using molecular dynamics, and then applying these parameters to simulate battery performance. We compare the results with those of standard Li-O batteries using PyBaMM software to gain insights into the potential advancements this molecule may offer.

II. MATERIALS AND METHODS

2.1. Design of the molecule

A new molecule with the molecular formula $C_6Li_6O_3$ was designed using ChemDraw, and the corresponding SMILES string "LiC1C(Li(O))C(Li)C(Li(O))C(Li)C1(Li(O))" was used to generate a.pdb file with a Python program. Using RDKit, the SMILES string was converted into a 3D PDB file format. Initially, the SMILES string was transformed into a molecular structure, hydrogens were added, and 3D coordinates were generated using the ETKDG algorithm. The resulting 3D molecular structure was then saved in PDB format for further analysis. Key lines of the program are provided below:

```
mol = Chem.AddHs(Chem.MolFromSmiles(smiles))
# Convert SMILES and add hydrogens
```

AllChem.EmbedMolecule(mol, AllChem.ETKDG()) # Generate 3D coordinates
Chem.MolToPDBFile(mol, pdb_filename) # Save as PDB file

This .pdb file was used to generate various physical parameters using various molecular dynamics methods. The chemical structure is shown in Figure1.

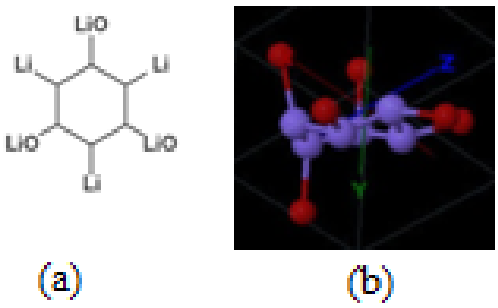

Figure-1: a) Chemical stucture of Li_6O_6 [15]; b) Chemical structure of $C_6Li_6O_3$

2.2. Methods

An input file for the General Utility Lattice Program (GULP) [16] was created using the fractional coordinates of atoms in the molecule $C_6Li_6O_3$, along with the parameters necessary for the Buckingham potential. Refinements were made until convergence was achieved, ensuring a stable molecular structure, which was confirmed by constructing spatial variations in the moduli using ElATE software [17]. The computed parameters from this method include heat capacity, zero-point energy, lattice and self-energy, elastic constants, dielectric constant (static), refractive index, P- and S-wave velocities, Young's modulus, bulk modulus, linear modulus, Poisson's ratio, phonon density, entropy, Helmholtz free energy, electro-negativity, electrostatic potential, and electric field gradients at atomic positions, as listed in Table 1.

Using Gaussian statistics and the WebMO platform [18], we simulated the IR and UV-Vis spectra of the $C_6Li_6O_3$ molecule, also calculating the dipole moment (see Table 1). Further, an input file for LAMMPS [20] was generated using Visual Molecular Dynamics (VMD) [19] to compute key battery parameters, such as electrolyte conductivity, electrolyte diffusivity, separator thermal conductivity, separator Bruggeman coefficient, separator specific heat capacity, and electrolyte viscosity, with values presented in Table 1.

Table 1: Physical parameters of $C_6Li_6O_3$ along with standard Lithium electrolyte.

Electrolytes (Approximate values as in references [1-3])	$C_6Li_6O_3$	Parameters (References [21-23])
Lattice energy (eV)	-3.08	80 kJ/mol
Zero point energy (eV)	0.383	0.2
Entropy (eV/K)	0.0335	50 J/mol-K
Helmholtz free energy	-9.77 eV	800 kJ/mol
Cv	51.10 cal/mol-K	50.0 J/mol-K
Dielectric constant (static)	1.13	6
Elastic Constants (GPa)	C_{11}=1.33 C_{12}= -0.575 C_{44}=0.965	C_{11}=200 C_{12}=80 C_{44}=70
Young's Modulus (GPa)	1.08	160
Bulk Modulus (GPa)	9.58	90
Poisson's ratio	0.623	0.25
Phonon Density of states	6-36 cm^{-1} 54-72 cm^{-1} 126-174 cm^{-1}	450-550 cm^{-1}
Electro-negativity (eV)	6.46	0.98
Self energy (eV)	-1.51	2.0
Dipole moment (Debye)	6.64	Low value
Electrolyte diffusivity ($m^2.s^{-1}$)	6.02e-8	5.2e-8
Separator Thermal conductivity ($W.m^{-1}.K^{-1}$)	2.6e-4	2.2e-6
Separator Bruggeman coefficient (electrolyte)	0.22	0.22
Separator specific heat capacity ($J.Kg^{-1}.K^{-1}$)	154.25	177.04
Electrolyte viscosity (Pa.s)	7.46e-10	3.0e-3
Electrolyte Density (g/cm^3)	3.0	1.2

Classical molecular dynamics (MD) simulations were carried out using the Large-scale Atomic/Molecular Massively Parallel Simulator (LAMMPS). Force field parameters derived from the OPLS-AA force field were applied to model interactions within the $C_6Li_6O_3$ matrix. The MD simulations provided insights into various properties of $C_6Li_6O_3$, including viscosity, surface tension, cohesive energy, degree of conversion, and glass transition temperature. For additional property calculations, GULP was used to determine physical parameters such as lattice energy and mechanical properties, leveraging classical force fields to assess the structural and energetic characteristics of the molecule.

Ab initio and quantum mechanical calculations were also performed via WebMO, using the Hartree-Fock (HF) method and LANL2DZ basis set to simulate

UV-Vis and IR spectra of the $C_6Li_6O_3$ system. These calculations offered insights into the electronic and optical properties of these materials.

III. RESULTS AND DISCUSSION

3.1. Characterisation parameters of $C_6Li_6O_3$

This section outlines the fundamental properties of the molecule, establishing its potential as an electrolyte.

Structural Properties: As shown in Table 1, the lattice point energy—representing the potential energy of an atom in the lattice due to neighboring interactions—ranges from -60 to -80 kJ/mol, which is comparable to that of standard Li_2O. The zero-point energy is around 0.2 eV, and the self-energy is approximately 2 eV, values typical for simple oxides like Li_2O.

Thermodynamic Properties: For standard Li_2O, the heat capacity is around 60 J/mol·K, entropy is 50 J/mol·K, and Helmholtz free energy is 800 kJ/mol. The values for the present material, provided in Table 1, align closely with these standards, suggesting thermodynamic stability.

Elastic and Mechanical Properties: As reported in Table 1, the Young's modulus, bulk modulus, and Poisson's ratio fall within ranges comparable to Li_2O, approximately 160 GPa, 110 GPa, and 0.25, respectively. These values are promising, as they suggest mechanical robustness suitable for electrolyte applications.

Optical Properties: Optical parameters for standard Li_2O, such as the dielectric constant (around 6), refractive index (approximately 1.75 for the sodium D-line), and phonon density peaks (450-455 cm^{-1}), are in general agreement with the values observed for this material (Table 1).

The spatial variations of Young's modulus, linear modulus, shear modulus, and Poisson's ratio are illustrated in Figure 2.

- Young's Modulus Plot: The shape and extent of the green surface in this plot reveal spatial variations in Young's modulus, indicating the material's stiffness distribution. The elongated form suggests an anisotropic structure, meaning stiffness varies by direction. Higher or well-distributed Young's modulus can enhance the electrolyte's mechanical stability, reducing the likelihood of mechanical failure under the stresses of battery cycling.
- Linear Modulus Plot: This plot shows the spatial variation in linear modulus, reflecting elasticity or stress-strain relationships in specific directions. A balanced variation in linear modulus aids the material's ability to retain structural integrity during lithium-ion migration, a critical factor for battery life and performance.
- Shear Modulus Plot: The blue regions with internal patterns display how the shear modulus, which measures resistance to shearing deformations, varies spatially. Higher shear modulus values indicate increased resistance to shape changes under load, helping to prevent electrode-electrolyte interface instability—a common issue in lithium-ion batteries—thereby enhancing cycling efficiency.
- Poisson's Ratio Plot: This plot depicts the material's tendency to expand or contract perpendicular to an applied stress. The complex surface structure suggests substantial spatial variation. A well-controlled and distributed Poisson's ratio enables the material to manage volumetric changes (e.g., during lithium intercalation) without forming cracks or voids, which would otherwise compromise battery performance.

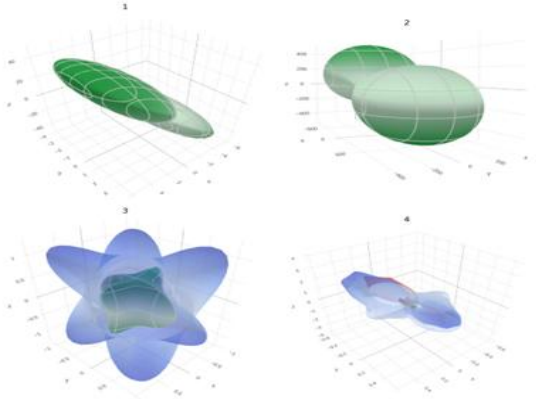

Figure-2: 1) Young's, 2) Linear, 3) Shear and 4) Poisson's spatial variations in $C_6Li_6O_3$

The electric field gradient (EFG) around lithium atoms provides insights into the mobility of lithium ions. A low and symmetric EFG indicates minimal restriction on ion movement, promoting higher mobility. Conversely, a high and anisotropic EFG suggests strong interactions with neighboring atoms, potentially limiting ion mobility. EFG also plays a role in the formation of the solid-electrolyte inter-

phase (SEI) layer, which can contribute to improved battery longevity. Figure 3 illustrates the variation of EFG alongside the potential distribution for $C_6Li_6O_3$.

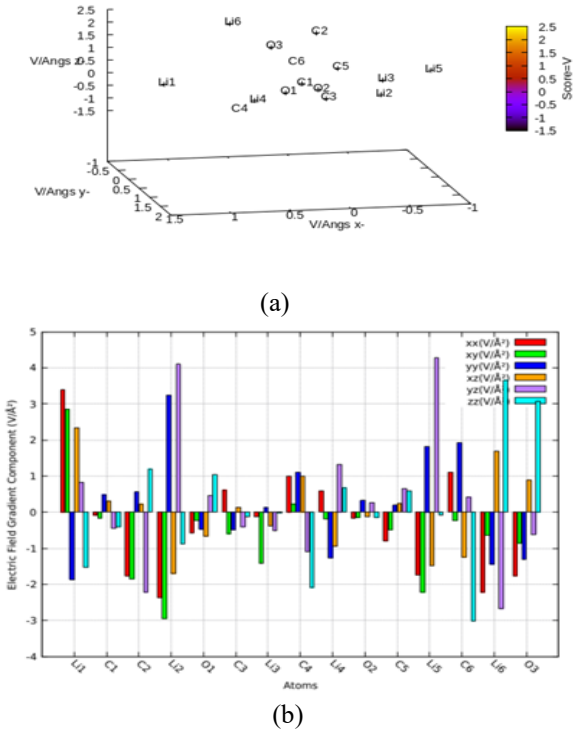

Figure 3: (a) Atomic portentals and (b) Electric Field gradient (EFG) for $C_6Li_6O_3$.

Computation of Bruggeman Coefficient [24]

The Bruggeman equation provides a model for calculating the effective dielectric constant of a composite material with multiple constituents, each characterized by its dielectric constant (ϵ_i) and volume fraction (f_i). The general form of the Bruggeman equation is: $\sum_i f_i\epsilon_i+2\epsilon_{eff}\epsilon_i-\epsilon_{eff} = 0$. Steps to Compute the Bruggeman Coefficient: 1) Define the dielectric constants of the constituents $\epsilon_1, \epsilon_2,\ldots\epsilon_n$, 2) Specify the volume fractions $f_1,f_2,\ldots f_n$, ensuring that $\sum f_i=1$ and 3) Solve the Bruggeman equation to find the effective dielectric constant ϵ_{eff}. This is typically done numerically because the equation is nonlinear.

In this study, a LAMMPS script computes the Bruggeman coefficient for the composite material, providing insights into the effective dielectric constant of the mixture. The script begins by defining simulation parameters, reading atomic data, applying force field interactions, and equilibrating the system using the NPT ensemble. Key steps include calculating the dielectric constants of both the matrix and dispersed phases, followed by the computation of the Bruggeman coefficient.

variable effective_dielectric_constant equal "(${internal_efield}/${applied_efield})" variable bruggeman_coefficient equal "(${effective_dielectric_constant}-${matrix_dielectric_constant})/(${effective_dielectric_constant}+2*${particle_dielectric_constant})/(${particle_dielectric_constant}-${matrix_dielectric_constant})/(${particle_dielectric_constant}+2*${matrix_dielectric_constant})"

Computation of Diffusion coefficient [25]

The diffusivity of ions in an electrolyte is an important parameter for understanding the transport properties of the electrolyte. The Nernst-Einstein equation is commonly used to calculate the diffusivity D of ions in an electrolyte. It relates the ionic conductivity σ, the concentration of ions c, and the diffusivity D. Here D describes how quickly ions diffuse through electrolyte.

Nernst-Einstein Equation: $D= s K_B T/ q_2 z_2 c$. Where: D: Diffusivity of the ion (m^2/s), σ: Ionic conductivity of the electrolyte (S/m), k_B: Boltzmann constant (1.38×10^{-23} J/K), T: Absolute temperature (K), q: Elementary charge (1.602×10^{-19} C), z: Charge number of the ion (e.g., z=1 for Li+) and c: Ion concentration in the electrolyte (m^{-3})

LAMMPS script file to compute diffusion coefficient

The simulation box is initialized from a data file, with atomic charges assigned to different ion types (Li^+ and O^-). The interaction potential is defined using a Lennard-Jones potential combined with long-range Coulombic interactions. Initial velocities are generated for all atoms at a specified temperature. The simulation then undergoes two equilibration phases: first, an NPT ensemble is used to stabilize pressure and density, followed by an NVT ensemble to maintain a constant temperature. After equilibration, the system transitions to the NVE ensemble for calculating the diffusion coefficient. The diffusion coefficient is computed based on the mean squared displacement (MSD) of ions, using the Einstein relation for diffusivity. The following commands were used.

variable D equal c_msd[4]/6/(step${dt}+1.0e-6)*${convert} print "average diffusion coefficient: $D"*

Electrolyte viscosity using LAMMPS [26]

The simulation setup includes defining the boundary conditions and atom style, loading atomic configurations from a data file, and specifying a Lennard-Jones potential with parameters suitable for Argon interactions. System equilibration and thermalization are performed under the NVT ensemble to reach the target temperature, with the option to switch to the NVE ensemble if required. For viscosity computation, the stress tensor components (p_{xy}, p_{xz}, p_{yz}) are sampled and correlated over time, applying the Green-Kubo relation to calculate viscosity. The following commands were used.

variable v equal (v_v11+v_v22+v_v33)/3.0 print "average viscosity: $v [Pa.s] @ $T K, ${ndens} atoms/A^3"

Thermal conductivity of $C_6Li_6O_3$

This LAMMPS script is designed to compute the thermal conductivity of a material by simulating atomic interactions and heat flux through molecular dynamics (MD) simulations. The script begins by initializing essential simulation parameters, setting the units to 'real' and defining the simulation box with periodic boundaries. Key variables are established, including temperature, time step, and system volume, along with conversion constants to obtain outputs in SI units. Atomic configurations are loaded from a data file, and an interatomic potential is specified using a Lennard-Jones potential with an appropriate cutoff for simulating atomic interactions. The masses of Lithium and Oxygen atoms are explicitly set, and the system is equilibrated under the NVT ensemble to stabilize the temperature before starting thermal conductivity calculations. Thermal conductivity is determined by measuring the heat flux and applying the Green-Kubo relation, which connects the autocorrelation of heat flux to conductivity. The following commands were used.

variable k equal (v_k11+v_k22+v_k33)/3.0 print "average conductivity: $k [W/mK] @ $T K, ${ndens} /A^3"

Specific heat capacity of $C_6Li_6O_3$

This Python program calculates the specific heat of the compound $Li_6O_3C_6$ based on the Dulong-Petit law [27], which approximates specific heat capacity as three times the gas constant, R, per mole. The program defines the atomic weights of each element in the compound and uses these values to compute the molar mass. This molar mass is then applied to convert the specific heat from a molar basis to a mass-specific basis (J/kg/K). The specific command lines are as follows:

*specific_heat_molar = 3 * R # Dulong-Petit specific heat in J/mol/K specific_heat_j_per_kg_k = specific_heat_molar / (molar_mass_g_per_mol / 1000) # Converted to J/kg/K*

Density of $C_6Li_6O_3$

This Python program calculates the density of a molecular structure defined in a .pdb file. It reads atomic coordinates and element types from the file to compute the molecular mass using predefined atomic weights. The program then calculates the volume of the bounding box surrounding the molecule to determine its density.

molecular_mass = calculate_molecular_mass(atoms) density = molecular_mass / volume # g/cm^3

Thermal conductivity is an important property for battery electrolytes, with Li_2O showing a value of 6 W/m·K, close to the value observed here for $C_6Li_6O_3$. Regarding electrical and conductive properties, the electrolyte conductivity of Li_2O (1.0 S/m) and the lithium-ion diffusivity (10^{-5} cm²/s) are slightly higher or lower when compared to the corresponding values for $C_6Li_6O_3$. Typical battery-specific parameters for Li_2O include separator thermal conductivity (0.3 W/m·K), the separator Bruggeman coefficient representing tortuosity in porous separators (1.5), separator specific heat capacity (1.2 J/g·K), and electrolyte viscosity (2 cP). These parameters are compared to the values obtained for $C_6Li_6O_3$ when simulating battery properties. Common electrolytes in lithium-ion batteries include polymer gels, ionic liquids, and ceramics.

The inherent electrochemical properties of $C_6Li_6O_3$, combined with these parameters, contribute to its enhanced performance as an electrolyte in lithium battery applications. Battery simulations for the $C_6Li_6O_3$ electrolyte were carried out using PyBaMM (Python Battery Mathematical Modeling), an open-source software designed for simulating battery behavior. PyBaMM provides a flexible framework for modeling various battery chemistries, particularly lithium-ion batteries, enabling analysis of battery performance, thermal effects, degradation

mechanisms, and electrochemical properties. The software includes pre-built models but also allows users to customize models and equations for specific battery designs. It is widely used to evaluate critical parameters, such as charge/discharge cycles, capacity fade, and electrolyte performance, making it a powerful tool for battery research and development.

We simulated both standard lithium-based battery properties and our new electrolyte, $C_6Li_6O_3$, with computed parameters, as shown in Figure 4(a, b and c)

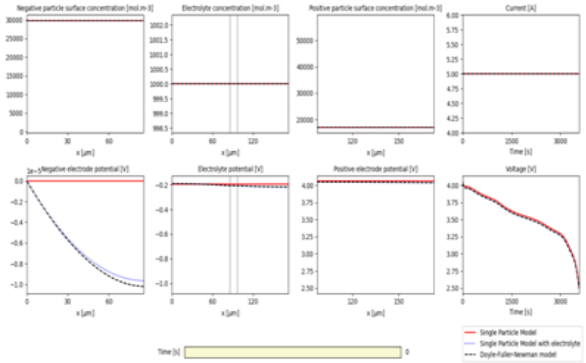

Figure 4(a) starting point at time = 0 hr for both standard and $C_6Li_6O_3$

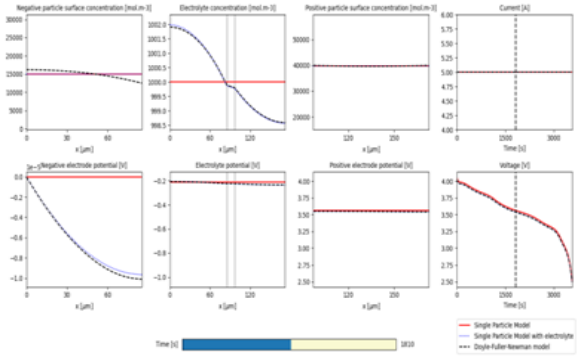

Figure 4(b) starting point at time =0.5hr for both standard and $C_6Li_6O_3$

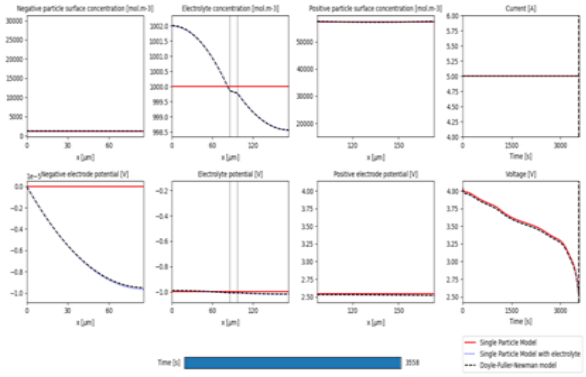

Figure 4(c) starting point at time =1hr for both standard and $C_6Li_6O_3$

For a better understanding of the battery properties like Voltage-capacity, current-time, Voltage-Time for both standard and $C_6Li_6O_3$ are given in Figure 5(a,b and c).

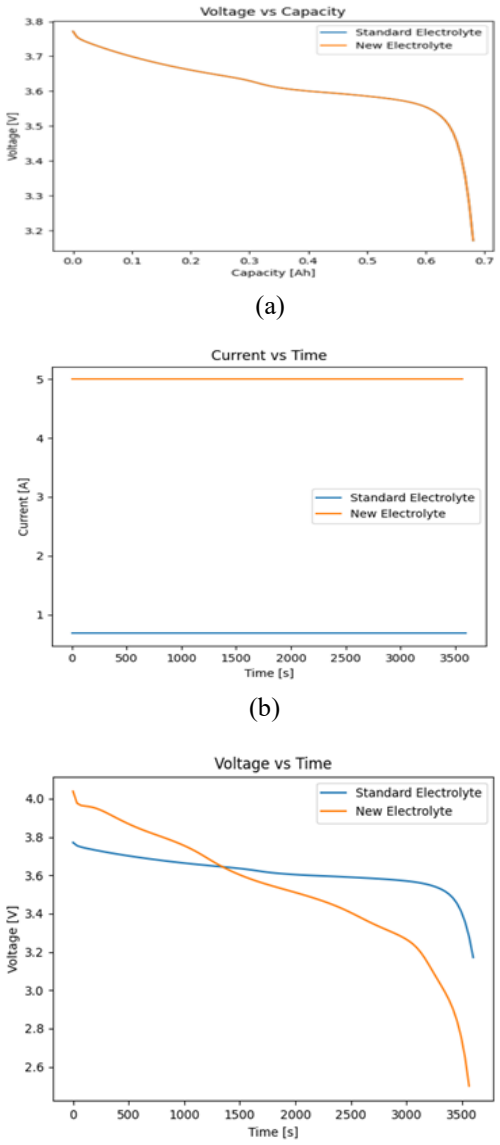

Figure 5: a) Voltage-time, b) Current-time and c) Voltage-time variations for $C_6Li_6O_3$ (red) and standard (blue).

In analyzing the comparison between the standard lithium-based electrolyte and the newly developed $C_6Li_6O_3$ electrolyte, the figures provided offer crucial insights into the performance characteristics of both materials. Below is a brief impact analysis based on the graphs:

1. Voltage vs. Time: The new electrolyte exhibits a

higher initial voltage but experiences a more rapid decline compared to the standard electrolyte. This suggests that, while the new electrolyte initially provides superior voltage performance, its stability over time may need further optimization. The observed drop could indicate faster degradation or reduced efficiency over prolonged time intervals. However, the higher initial voltage is promising for applications requiring a strong initial energy output.

2. Voltage vs. Capacity: The voltage-capacity graph shows the new electrolyte achieving a significantly higher capacity (around 5 Ah) compared to the standard electrolyte (which falls below 1 Ah). This indicates the superior energy storage capability of $C_6Li_6O_3$, making it suitable for high-capacity applications such as electric vehicles and large-scale energy storage systems. However, the sharp decline in voltage as capacity increases suggests potential challenges in maintaining stable voltage at higher capacities.

3. Current vs. Time: The new electrolyte sustains a higher current (around 5 A) consistently over time, while the standard electrolyte maintains a much lower current (around 1 A). This implies that $C_6Li_6O_3$ can support higher current densities, which is advantageous for high-power applications. Its ability to maintain current stability over time is also a critical feature for long-term use in practical devices.

The analysis reveals that the newly developed $C_6Li_6O_3$ electrolyte outperforms the standard lithium-based electrolyte in terms of both capacity and current stability. However, the faster voltage drop over time is a potential concern that may require further investigation. With its high capacity and current stability, this electrolyte shows promise for high-energy and high-power applications, strengthening its case for acceptance in the scientific community. Emphasizing these improvements in the paper will position the new electrolyte as a competitive alternative in the energy storage field.

IV. CORRELATION STUDIES

The correlation factor (or correlation coefficient) quantifies the strength and direction of the linear relationship between two variables. The most common measure is the Pearson correlation coefficient, which ranges between -1 and 1. Given two variables, X and Y (such as two columns in your dataset), the Pearson correlation coefficient r is calculated as:

$$r = \sum_{i=1}^{n} (X_i - X_{av})(Y_i - Y_{av}) / \text{sqrt}\left(\sum_{i=1}^{n} (X_i - X_{av})^2\right) \times \left(\sum_{i=1}^{n} (Y_i - Y_{av})^2\right).$$

Here X and Y are the values of the i^{th} observations of X and Y and X_{av} and Y_{av} are the mean values of X and Y, n is the number of observations. 3D representation of Correlation coefficient surface between the parameters across all the pairs for new and standard electrolytes is given in Figure 6(a) for standard electrolyte and 6(b) for $C_6Li_6O_3$ electrolyte.

Figure 6 indicates uniform highly correlated parameters in a positive manner with a value lying near +1.

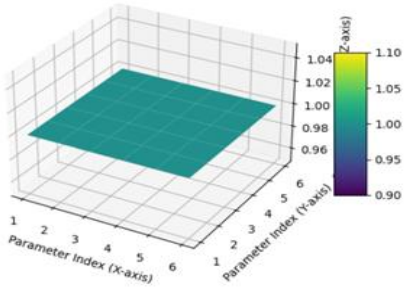

(a)

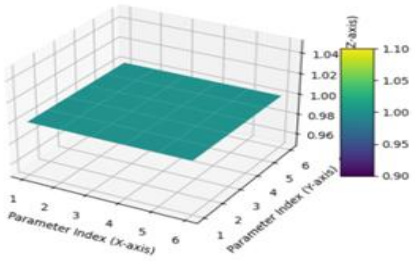

(b)

Figure 6: a) Correlation surface for standard Electrolyte parameters and b) for $C_6Li_6O_3$ parameters.

V. CONCLUSION

Following conclusions emerge from our study on $C_6Li_6O_3$[28]

1. Enhanced Energy Capacity: The $C_6Li_6O_3$ electrolyte demonstrates significantly higher energy storage capacity, as seen in the voltage versus capacity graph. This makes it highly suitable for applications requiring extended energy delivery, such

as electric vehicles and large-scale energy storage systems.

2. Superior Current Support**:** The ability of the $C_6Li_6O_3$ electrolyte to sustain higher current densities over time compared to the standard electrolyte suggests its suitability for high-power applications. This positions it as a favorable candidate for fast-charging technologies and devices requiring substantial power output without compromising battery longevity.

3. Initial Voltage Boost**:** The higher initial voltage provided by $C_6Li_6O_3$ indicates its potential to deliver a more powerful start-up performance, which can be advantageous in applications that demand rapid initial energy release. However, the faster voltage decline observed over time highlights a potential trade-off between immediate performance and long-term stability.

4. Physical Parameter Advantages: Beyond just battery performance, the physical parameters such as cohesive energy, surface tension, and viscosity for $C_6Li_6O_3$ align well with the requirements for solid-state electrolytes, offering better thermal stability and ionic conductivity. These characteristics improve battery safety and longevity, particularly in harsh operating conditions.

5. Opportunities for Optimization**:** While $C_6Li_6O_3$ shows clear advantages in capacity and current support, the faster voltage drop and potential for rapid degradation over extended cycles indicate that further optimizations are needed. Addressing these issues through potential doping strategies or structure modification could improve long-term stability and overall efficiency.

6. The new $C_6Li_6O_3$ electrolyte offers substantial improvements in energy capacity and current density compared to standard lithium-based electrolytes, making it an attractive option for next-generation energy storage systems. Its superior performance, particularly in high-capacity and high-power applications, positions it as a competitive alternative in the development of advanced batteries. While there is a need to address the observed voltage stability over time, these initial results are promising, and further optimizations could unlock its full potential, enhancing both the safety and efficiency of future energy storage solutions.

7. Correlation value lies near +1 for both standard and $C_6Li_6O_3$ electrolytes indicating there is a uniform high correlation among the parameters.

A procedure to synthesis this compound is We have identified a method to do this and it is “Dissolve cyclohexane-1,2,3-triol in dry THF or hexane under an inert atmosphere. Cool the solution to -78°C using a dry ice-acetone bath. Slowly add n-BuLi or LDA solution dropwise to the cooled mixture. After the addition is complete, allow the reaction to proceed for the required time (typically 1-2 hours) at -78°C. Gradually warm the mixture to room temperature. For Isolation, Quench the reaction by careful addition of methanol or water to neutralize any unreacted lithium reagent. Extract the product with diethyl ether. Dry the organic phase over anhydrous magnesium sulfate. Filter and concentrate the solution under reduced pressure. Figure 7 shows graphical representation of the process.

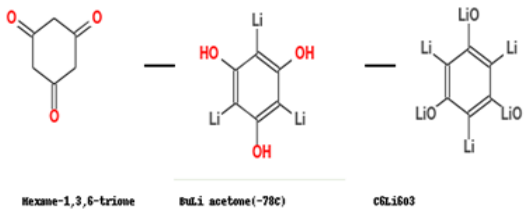

Figure 7: Probable Reaction procedure for the synthesis of $C_6Li_6O_3$

VI. ACKNOWLEDGEMENTS

We have not received any funds for this research. We acknowledge encouragement from our institutions for carrying out research.

REFERENCES

[1] G. Jiang, J. Liu, J. He, H. Wang, S. Qi, J. Huang, D. Wu and J. Ma, - Hydrofluoric Acid-Removable Additive Optimizing Electrode Electrolyte Interphases with Li^+ Conductive Moieties for 4.5 V Lithium Metal Batteries, Adv. Funct. Mater., vol. 33(12), pp 2214422(1-10), 2023.

[2] X.B. Cheng, R. Zhang, C.Z. Zhao and Q. Zhang, -Toward Safe Lithium Metal Anode in Rechargeable Batteries- A Review, Chem. Rev., vol.117, pp 10403–10473, 2017.

[3] D. Lin, Y. Liu, and Y. Cui, - Reviving the lithium metal anode for high-energy batteries, Nat. Nanotechnol, vol.12 (3), pp194–206, 2017.

[4] G. Zheng, S.W. Lee, Z. Liang, H.W. Lee, K. Yan, H. Yao, H. Wang, W. Li, S. Chu, and Y. Cui, - Interconnected hollow carbon nanospheres for stable lithium metal anodes, Nat. Nanotechnol., vol.9(8) pp618–623, 2014.

[5] Y. Wang, Z. Li, Y. Hou, Z. Hao, Q. Zhang, Y. Ni, Y. Lu, Z. Yan, K. Zhang, Q. Zhao,F. Li, and J. Chen, - Emerging electrolytes with fluorinated solvents for rechargeable lithium-based batteries, Chem. Soc. Rev., vol.52(8), pp2713–2763, 2023.

[6] C. Yan, Y.X. Yao, X. Chen, X.B. Cheng, X.Q. Zhang, J.Q. Huang, and Q. Zhang, - Lithium Nitrate Solvation Chemistry in Carbonate Electrolyte Sustains High-Voltage Lithium Metal Batteries, Angew. Chem. Int. Ed. Engl., vol.57(43), pp14055–14059, 2018.

[7] J. Fu, X. Ji, J. Chen, L. Chen, X. Fan, D. Mu, and C. Wang, - Lithium Nitrate Regulated Sulfone Electrolytes for Lithium Metal Batteries, Angew. Chem. Int. Ed. Engl., vol.59(49), pp22194–22201, 2020.

[8] John C. Hewson, Hanwei Zhou, Mukul Parmananda, Randy C. Shurtz and Partha P. Mukherjee, - From material properties to multiscale modeling to improve lithium-ion energy storage safety, MRS Butlletin, vol.46, pp402-409, 2021.

[9] Wei Wei and Xingang Yu,- Molecular dynamics study of the effect of lithium on the tensile behaviors of bcc iron, Materials Today Communications 24, pp101217, 2020.

[10] Yang Huang, Long Liu and Min Gao, - Molecular dynamics study on the Li diffusion mechanism and delithiation process of Li_2MnO_3, Solid State Ionics, vol.346, pp115195, 2020.

[11] Ajay Muralidharan, Mangesh I. Chaudhari, Lawrence R. Pratt and Susan B. Rempe, - Molecular Dynamics of Lithium-Ion Transport in a Model Solid Electrolyte Interphase, Scientific Reports, vol.8, pp10736, 2018 | DOI:10.1038/s41598-018-28869-x.

[12] Selva Chandrasekaran Selvaraj, Volodymyr Koverga, and Anh T. Ngo, - Exploring Li-Ion Transport Properties of Li_3TiCl_6: A Machine Learning Molecular Dynamics Study, Journal of The Electrochemical Society, vol.171, pp050544, 2024.

[13] Y. Mabrouk, N. Safaei, F. Hanke, J. M. Carlsson, D. Diddens and A. Heuer, - Reactive molecular dynamics simulations of lithium-ion battery electrolyte degradation, Scientific Reports, vol.14, pp10281, 2024.

[14] Koki Nakano, Naoto Tanibata, Hayami Takeda, Ryo Kobayashi, Masanobu Nakayama and Naoki Watanabe, - Molecular Dynamics Simulation of Li-Ion Conduction at Grain Boundaries in NASICON-Type $LiZr_2(PO_4)_3$ Solid Electrolytes, J. Phys. Chem. C, vol.125, pp23604−23612, 2021.

[15] V.V. Manju, Sumana Y.K, K. M. Lokanatha Rai, N.K.Lokanath, U. Shilpa, and R. Somashekar,- Synthesis, Structure, Elastic, Electric and Charge Storage Capacity of Li_6O_6 Crystals, Biointerface Research in Applied chemistry, vol.13(2), pp180-196, 2022.

[16] J.D.Gale,- GULP A computer program for the symmetry-adapted simulation of solids, J.Chem Society-Faraday Transactions, vol.93, pp629-637, 1997.

[17] R.Gaillac, P.Pullumbi, F.X. Coudert, - ELATE: an open-source online application for analysis and visualization of elastic tensors, Journal of Physics: Condensed Matter, vol.28, pp275201,2016. https://doi.org/10.1088/0953-8984/28/27/275201.

[18] Polik, WF, Schmidt, JR, - WebMO: Web-based computational chemistry calculations in education and research, Comput Mol Sci., e1554 (2021). https://doi.org/10.1002/wcms.1554.

[19] Humphrey W., Dalke A. And Schulten K., - VMD: Visual molecular dynamics, J.Mole.Graphics, vol.14(1), pp33-38, 1996.

[20] A. P. Thompson, H. M. Aktulga, R. Berger, D. S. Bolintineanu,W. M. Brown, P. S. Crozier, P. J. , Veld, A. Kohlmeyer, S. G. Moore, T. D. Nguyen, R. Shan,M. J. Stevens, J. Tranchida, C. Trott, and S. J. Plimpton,- LAMMPS - a flexible simulation tool for particle-based materials modeling at the atomic, meso, and continuum scales, Comp. Phys. Comm., 271, pp10817, 2022.

[21] Mohsen Sotoudeh, Sebastian Baumgart, Manuel Dillenz, Johannes Döhn, Katrin Forster-Tonigold, Katharina Helmbrecht, Daniel Stottmeister, and Axel Groß, - Ion Mobility in Crystalline Battery Materials, Adv. Energy Mater., vol.14, pp2302550(1-29), 2024.

[22] K. Xu, - Nonaqueous liquid electrolytes for lithium-based rechargeable batteries, Chem. Rev., vol.104, pp4303−4417, 2004.

[23] Lizhen Long, Shuanjin Wang, Min Xiao and Yuezhong Meng, - Polymer electrolytes for lithium polymer batteries, J. Mater. Chem. A, vol.4, pp10038–10069, 2016.

[24] Y. M. Poon and F. G. Shjin,- A Simple Explicit Formula for Effective Dielectric Constant of Binary 0–3 Composites, Journal of materials science, vol.39, pp1277 – 1281, 2004.

[25] Xinying Lu,- Application of the Nernst-Einstein equation to concrete, Cement and Concrete Research, vol.27(2), pp293-302, 1997.

[26] Mohamed Mouas, Jean-Georges Gasser, Slimane Hellal and Benoît Grosdidier, - Diffusion and viscosity of liquid tin: Green-Kubo relationship-based calculations from molecular dynamics simulations, The Journal of chemical physics, vol.136, pp094501, 2012

[27] P Rosa and A Souza, - Dulong-Petit's law and Boltzmann's theoretical proof from the Kinetic Theory of Gases, Journal of Physics: Conference Series, vol.2727, pp012009, 2024. IOP Publishing doi:10.1088/1742-6596/2727/1/012009

[28] Mauger, A; Julien, C.M, - Critical Review on Lithium-Ion Batteries: Are They Safe? Sustainable? Ionics. Vol.23(8), pp1933–1947, 2017. doi:10.1007/s11581-017-2177-8